Article

Black-hole-triggered star formation in the dwarf galaxy Henize 2-10

https://doi.org/10.1038/s41586-021-04215-6

Received: 29 June 2021

Accepted: 8 November 2021

Published online: 19 January 2022

Check for updates

Zachary Schutte[1]✉ & Amy E. Reines[1]

Black-hole-driven outflows have been observed in some dwarf galaxies with active galactic nuclei[1], and probably play a role in heating and expelling gas (thereby suppressing star formation), as they do in larger galaxies[2]. The extent to which black-hole outflows can trigger star formation in dwarf galaxies is unclear, because work in this area has previously focused on massive galaxies and the observational evidence is scarce[3–5]. Henize 2-10 is a dwarf starburst galaxy previously reported to have a central massive black hole[6–9], although that interpretation has been disputed because some aspects of the observational evidence are also consistent with a supernova remnant[10,11]. At a distance of approximately 9 Mpc, it presents an opportunity to resolve the central region and to determine if there is evidence for a black-hole outflow influencing star formation. Here we report optical observations of Henize 2-10 with a linear resolution of a few parsecs. We find an approximately 150-pc-long ionized filament connecting the region of the black hole with a site of recent star formation. Spectroscopy reveals a sinusoid-like position–velocity structure that is well described by a simple precessing bipolar outflow. We conclude that this black-hole outflow triggered the star formation.

Radio observations of Henize 2–10 using very long baseline interferometry reveal a nuclear, compact, non-thermal source with a luminosity of $L_R \sim 4 \times 10^{35}$ erg s^{-1} and a physical size <3 pc × 1 pc (ref. [7]). High-resolution X-ray observations unveil a point source with $L_X \sim 10^{38}$ erg s^{-1} that is spatially coincident with the compact nuclear radio source[8]. There are two possible explanations for these radio and X-ray observations alone—a highly sub-Eddington massive black hole (that is, a low-luminosity active galactic nucleus (AGN)) or a very young supernova remnant[7,10]. However, there are other observational results to consider regarding the origin of the nuclear radio/X-ray source in Henize 2-10. We summarize these results in Extended Data Table 1 and demonstrate that a highly sub-Eddington massive black hole is consistent with all the available observations including the results presented here, whereas a supernova remnant is not.

We observed Henize 2-10 at optical wavelengths using the Space Telescope Imaging Spectrograph (STIS) on the Hubble Space Telescope (HST). We obtained observations of the central regions of Henize 2-10 with the 0.2"-slit in two orientations. The first, referred to as the east–west (EW) orientation, is centred on the nuclear radio/X-ray source and aligned with the filamentary ionized structure between the two bright, extended regions of ionized gas previously identified in narrowband Hα imaging with HST[6] (Fig. 1). The second, referred to as the North–South (NS) orientation, is centred on the nuclear source and rotated 90° with respect to the EW observation. We obtained high-dispersion observations (velocity resolution of approximately 40 km s^{-1}) at both slit positions using the G750M and G430M gratings, which cover the strong emission lines of interest (for example, Hα, [N II], [S II], [O I] and Hβ, [O III], respectively).

The kinematics of the ionized gas provide evidence for an outflow originating from a nuclear massive black hole. First, we detect substantially broadened emission lines at the location of the central source in both slit orientations. In particular, the [O I]6300 emission line has a broad component with a full-width at half-maximum (FWHM) of 497 km s^{-1} as measured in the EW slit (and 445 km s^{-1} in the NS slit) using a 3-pixel extraction region in the spatial dimension. Although the [O I] line is too weak to be detected all along the EW filament (or NS slit), it is detected at the location of the bright star-forming region of approximately 70 pc to the east with a FWHM = 103 km s^{-1}, which is much less than that of the central source (for example, see top left panel of Fig. 2). The [O III]5007 line is much stronger than [O I]6300 and detectable all along the EW filament. The FWHM of the broad component of [O III] at the location of the nuclear source is 271 km s^{-1}, which is somewhat broader than the median value per spatial pixel along the EW slit (175 km s^{-1} with a s.d. of 53 km s^{-1}). We do not observe such broad emission beyond the location of the central source in the NS slit (Fig. 2, top right). We emphasize that the line widths at the location of the nuclear source are consistent with a low-velocity outflow from a massive black hole, but would be anomalously low for a very young supernova remnant with typical FWHMs of thousands of km s^{-1} (refs. [13,14]).

In addition to broadened emission lines at the location of the central source, we also find Doppler-shifted velocities along the EW slit that exhibit a coherent sinusoid-like pattern that is relatively smooth, especially in comparison to the position–velocity diagram along the NS slit orientation that shows no evidence of a coherent pattern in the Doppler velocities of strong emission lines (Fig. 2 and Methods). Moreover, a simple model of a precessing bipolar outflow broadly reproduces the

[1]eXtreme Gravity Institute, Department of Physics, Montana State University, Bozeman, MT, USA. ✉e-mail: zachary.schutte@montana.edu

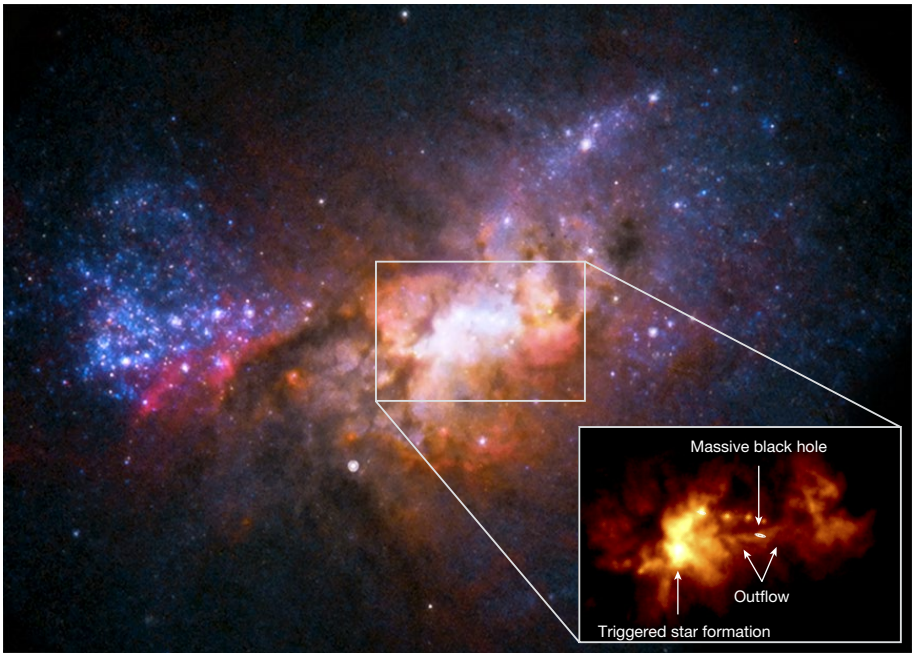

Fig. 1 | HST optical image of the dwarf starburst galaxy Henize 2-10. The inset shows a narrowband Hα+continuum image of the central 6" × 4" region. At the distance of Henize 2-10 (approximately 9 Mpc), 1" corresponds to approximately 44 pc. White contours indicate compact radio emission detected with very long baseline interferometry and mark the location of the central massive black hole[7], which is also detected in X-rays[8]. Our HST spectroscopy demonstrates that the black hole is driving an outflow that is triggering the formation of young, massive star clusters. The main image is 25" (approximately 1.1 kpc) across. Credit: NASA/STScI.

observed sinusoid-like velocity pattern along the EW slit that is aligned with the ionized filament seen in narrowband Hα imaging with HST (see Methods for a description of the model). Precessing jets have been observed in many AGNs, although they are typically found in more luminous quasars and radio galaxies[15,16]. Theories for the origin of precessing jets and/or outflows include accretion disk warping, jet instabilities and the presence of massive black-hole binaries[17,18]. However, the coherent velocity pattern we observe over approximately 150 pc along the ionized filament centred on the central source is incompatible with a supernova-remnant origin because supernova remnants do not drive quasi-linear outflows on such large scales.

There is also evidence that the black-hole outflow is triggering the formation of star clusters in the central region of Henize 2-10. HST imaging shows that the ionized filament extends eastwards from the massive black hole to a bright knot of ionized gas that is the site of recent star formation located 1.5" (approximately 70 pc) away from the black hole (Fig. 3). Given that our HST spectroscopy along this filament exhibits a continuous velocity pattern, which can be tracked from the black hole to the eastern star-forming region and is well described by a precessing bipolar outflow model, this strongly suggests that the outflow driven by the black hole is causally connected to the region of recent star formation. There is also a secondary, blue-shifted peak (offset by 154 km s^{-1}) detected in the emission lines at the location of the bright star-forming knot, suggesting that the outflow is pushing the line-emitting gas clouds and influencing their kinematics (Fig. 3). The double-peaked lines would naturally arise as the outflow intercepted dense gas and primarily pushed it in the lateral direction rather than ahead of the flow. The handful of young star clusters associated with the star-forming knot have ages of approximately 4 Myr (Methods) and are predominately aligned in the north–south direction, which is consistent with a scenario in which they formed from gas moving in opposite directions owing to the effect of the black-hole outflow[19]. There is also a local peak in the gas density at the location of the star-forming knot with $n_e \gtrsim 10^4$ cm^{-3} (Extended Data Fig. 3), consistent with the outflow compressing gas clouds and enhancing star formation in this region. It is notable that we also detect double-peaked emission-line profiles to the west of the massive black hole at the boundary of a dark cloud of gas and dust (region 5, see Extended Data Fig. 4), suggesting that the other side of the bipolar outflow is also intercepting dense clouds and pushing them in a direction perpendicular to the outflow direction. Just to the west of this region (region 6, Extended Data Fig. 4), the equivalent width of the Hα emission line indicates stellar ages $\lesssim$3 Myr, indicating a very early stage of star formation in which the infant star clusters have not had enough time to destroy or disperse the dense molecular gas from which they formed, leading to high levels of extinction[20].

The ionization conditions of the gas provide additional support for a massive black hole with an outflow. First, our HST spectroscopy at approximately 0.1" resolution clearly reveals non-stellar ionization at the location of the central source based on the flux ratio of [O I]/Hα, which is consistent with gas photoionized by an accreting massive black hole (Extended Data Fig. 5). Additionally, supernova remnants are known to be strong [S II] emitters with log [S II]/Hα > −0.5 (ref. [21]), which is not seen in the STIS spectrum of the nuclear source. The ionization conditions probed by optical diagnostics using [O III]/Hβ versus [N II]/Hα and [S II]/Hα do not clearly indicate a (luminous) AGN, which at first glance may seemingly rule out the presence of a massive black hole. However, there are a number of potential reasons for this apparent discrepancy. First, [N II] and [S II] are not as sensitive to the hardness of the ionizing radiation field as [O I] and are therefore less reliable at identifying AGNs. Second, the massive black hole in Henize 2-10 is accreting at a tiny fraction of its Eddington luminosity (approximately $10^{-6} L_{Edd}$)[8], which can affect the emission lines so that they do not look like those of luminous AGNs with higher Eddington ratios[22]. The apparent contradiction of emission-line diagnostics can also arise when there is underlying star formation contributing to the spectrum. Finally, we note that there are other examples of radio-selected massive black holes in dwarf galaxies with enhanced [O I] that do not look like optical AGNs in the other diagnostic diagrams[23,24].

We also find that the ionization conditions probed by strong emission-line ratios at the location of the central source and along the

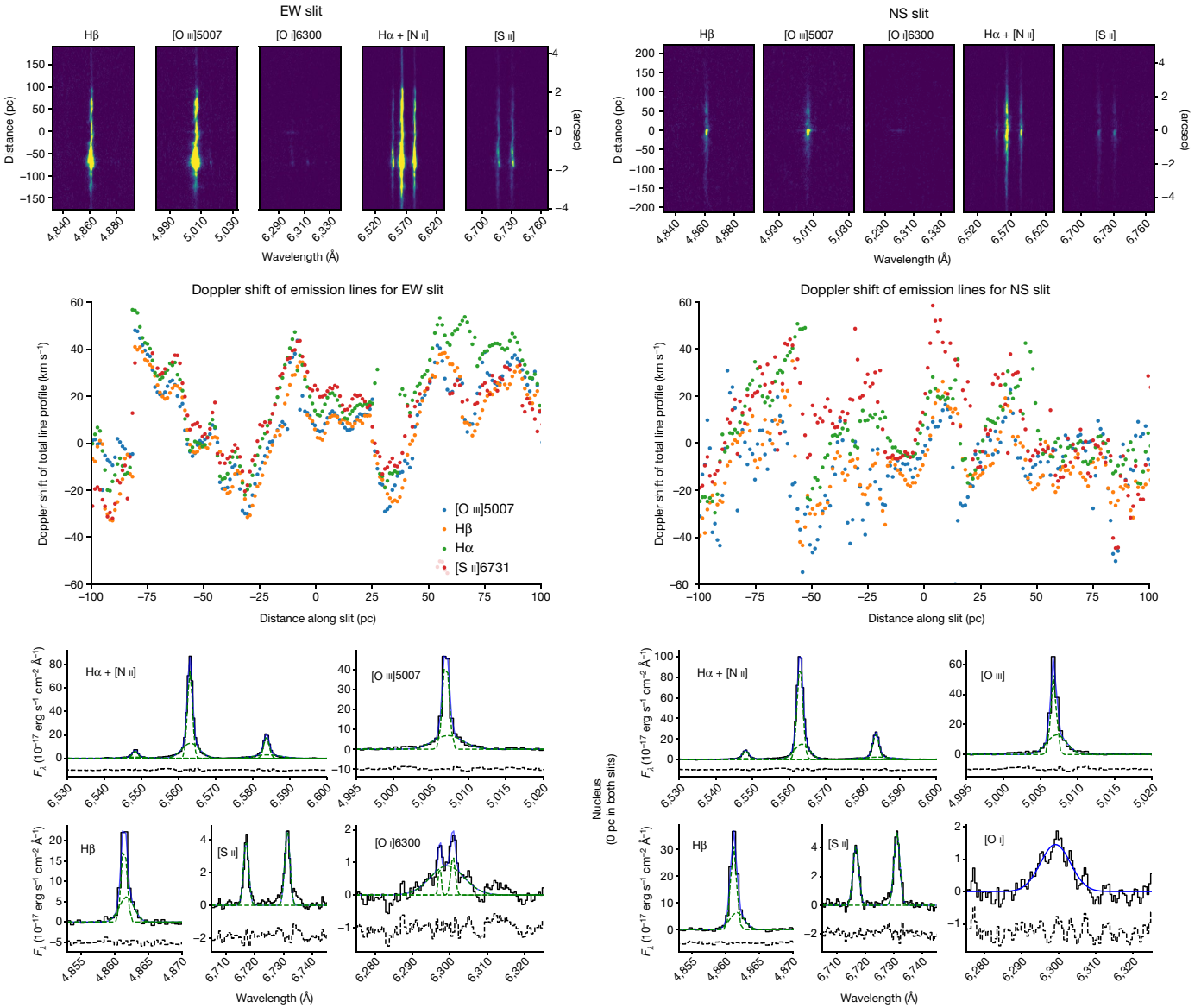

Fig. 2 | Optical spectra and ionized gas kinematics for the central region of Henize 2-10. The top panels show 2D continuum-subtracted HST STIS spectra of key emission-line regions along the EW and NS slit orientations. The middle panels show position–velocity diagrams along each slit position where Doppler shifts are relative to the systemic velocity of the galaxy (873 km s^{-1})[12]. The velocity pattern in the EW slit is much more coherent than that in the NS slit. The bottom panels show extracted one-dimensional spectra (expressed in units of flux density, F_λ) at the location of the nuclear massive black hole. The region surrounding the nucleus (0 pc in both slit positions) shows strong broadened emission lines, including [O I]6300 and [O III]5007.

filament are well described by theoretical models of shocks propagating in a high-density medium[25] (Methods). Specifically, emission-line ratios in the central region of approximately 150 pc along the EW slit orientation are consistent with models of a shock with a velocity of approximately 200 km s^{-1} travelling through a gas with an electron density of approximately 1,000 cm^{-3}, and include a 'precursor' model component of ionizing photons that travel upstream from the shock front pre-ionizing the gas. The model shock velocities that match the strong emission-line ratios agree with those obtained from direct measurements of the line widths from our kinematic study described above (for example, [O III]), and the model gas densities are consistent with our measurements using the density sensitive line ratio [S II]6716/6731 (Methods). Moreover, these conditions are well explained by an AGN-driven outflow mechanically exciting the interstellar medium in these regions, in addition to the precursor component contributing to the photoionization of the interstellar medium. There is also evidence for shocked emission at the location of the eastern star-forming region, particularly from the secondary blue-shifted peak, in addition to photoionization from young hot stars (Methods). Combining these results with our kinematic study indicates that the bipolar outflow generated by the central black hole is shocking the interstellar medium in the central regions of Henize 2-10, creating conditions that are favourable for positive AGN feedback[26,27].

AGN-driven outflows have been discovered in a small sample of dwarf galaxies, although the discovery of a black-hole outflow in Henize 2-10, to our knowledge, provides the first example that is robustly spatially resolved. Moreover, Henize 2-10 differs from these other systems in several other ways. The majority of black-hole-driven outflows in dwarf galaxies have been found in galaxies with well-defined nuclei and optically selected AGNs with relatively high accretion rates. These observations suggest that the AGNs play a role in heating and expelling gas in the galaxies and quenching star formation, which is a phenomenon known as negative feedback[28]. This is in stark contrast with Henize 2-10, which has an irregular central morphology, is intensely forming

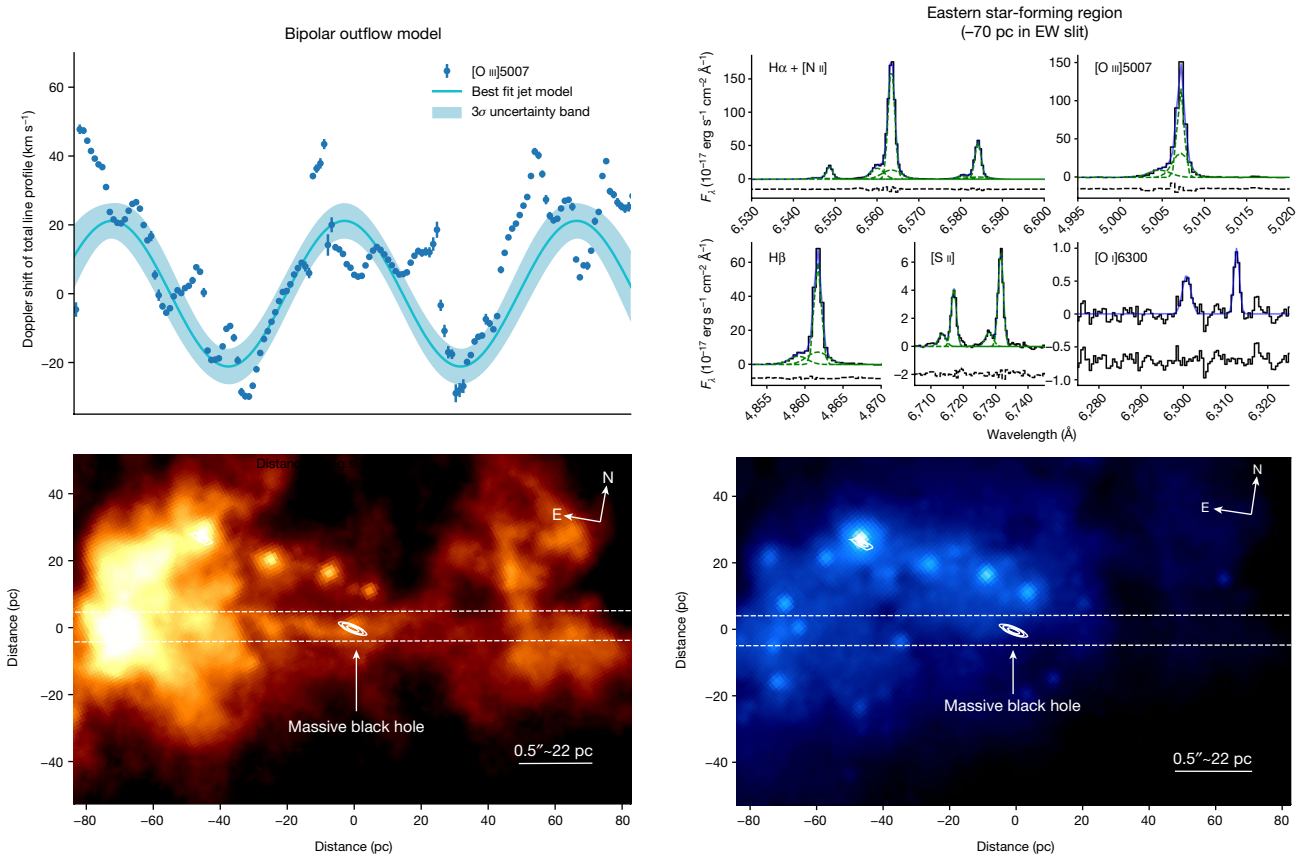

Fig. 3 | Visualization of the bipolar outflow model and star-forming regions. Top left, position–velocity diagram of the [O III]5007 emission line along the EW slit where the Doppler shifts are relative to the systemic velocity of the galaxy (873 km s^{-1})[12]. The data are well described by a simple precessing outflow model with a precession frequency of f ~ 5 revolutions Myr^{-1} and a precession angle of θ ~ 4° (Methods). Bottom left, HST narrowband Hα+continuum image showing that the EW slit position is aligned with the ionized filamentary structure connecting the massive black hole and the site of recent star formation approximately 70 pc to the east. White contours indicate compact radio emission from very long baseline interferometry[7] and show the location of the massive black hole. Bottom right, HST 0.8 μm (around the I-band) broadband image with the same field of view. Young star clusters in the eastern star-forming region are highlighted with an ellipse. Top right, spectra of the eastern star-forming region (–70 pc) show strong broad emission lines with a secondary blue-shifted peak most clearly visible in the [S II] emission.

stars and is experiencing positive feedback from a weakly accreting black hole that is luminous at radio, rather than optical, wavelengths.

Indeed, 'jet-mode' feedback is often associated with radio-loud AGNs accreting at low Eddington ratios, and is attributed to the unbound nature of radiatively inefficient accretion flows[22,29,30]. Warm ionized gas outflows are observed to accompany the radio jets and/or outflows in some cases, particularly in young radio galaxies in which nascent jets are expanding through the interstellar medium in the central regions of their hosts[30]. In these systems, the spatial extents of the warm outflows (traced by emission lines) are similar to the radio morphologies. A similar phenomenon is observed in Henize 2-10, which is most readily found in a comparison between the radio emission detected with the Very Large Array and Paα emission detected by HST in the central few hundred pc of the galaxy[6]. However, an important difference between Henize 2-10 and powerful young radio galaxies is that the emission lines are dominated by AGN photoionization in the more massive and luminous systems, whereas the extended emission-line regions in Henize 2-10 are dominated by star formation (enhanced and/or triggered by the black-hole outflow). Therefore, Henize 2-10 may be a low-mass, low-power analogue of young radio galaxies.

Online content

Any methods, additional references, Nature Research reporting summaries, source data, extended data, supplementary information, acknowledgements, peer review information; details of author contributions and competing interests; and statements of data and code availability are available at https://doi.org/10.1038/s41586-021-04215-6.

1. Manzano-King, C. M., Canalizo, G. & Sales, L. V. AGN-driven outflows in dwarf galaxies. *Astrophys. J.* **884**, 54 (2019).
2. Fabian, A. C. Observational evidence of active galactic nuclei feedback. *Annu. Rev. Astron. Astrophys.* **50**, 455–489 (2012).
3. Gaibler, V. et al. Jet-induced star formation in gas-rich galaxies. *Mon. Not. R. Astron. Soc.* **425**, 438–449 (2012).
4. Maiolino, R. et al. Star formation inside a galactic outflow. *Nature* **544**, 202–206 (2017).
5. Gallagher, R. et al. Widespread star formation inside galactic outflows. *Mon. Not. R. Astron. Soc.* **485**, 3409–3429 (2019).
6. Reines, A. E. et al. An actively accreting massive black hole in the dwarf starburst galaxy Henize 2-10. *Nature* **470**, 66–68 (2011).
7. Reines, A. E. & Adam, T. D. Parsec-scale radio emission from the low-luminosity active galactic nucleus in the dwarf starburst galaxy Henize 2-10. *Astrophys. J. Lett.* **750**, L24 (2012).
8. Reines, A. E. et al. Deep Chandra observations of the compact starburst galaxy Henize 2-10: X-rays from the massive black hole. *Astrophys. J. Lett.* **830**, L35 (2016).
9. Riffel, R. A. Evidence for an accreting massive black hole in He 2-10 from adaptive optics integral field spectroscopy. *Mon. Not. R. Astron. Soc.* **494**, 2004–2011 (2020).
10. Hebbar, P. R. et al. X-ray spectroscopy of the candidate AGNs in Henize 2-10 and NGC 4178: likely supernova remnants. *Mon. Not. R. Astron. Soc.* **485**, 5604–5615 (2019).
11. Cresci, G. et al. The MUSE view of He 2-10: No AGN ionization but a sparkling starburst. *Astron. Astrophys.* **604**, A101 (2017).
12. Kobulnicky, H. A. et al. Aperture synthesis observations of molecular and atomic gas in the Wolf-Rayet starburst galaxy. *Astron. J.* **110**, 116 (1995).
13. Mathewson, D. S. et al. A new oxygen-rich supernova remnant in the Large Magellanic Cloud. *Astrophys. J.* **242**, L73–L76 (1980).

14. Borkowski, K. J. et al. Asymmetric expansion of the youngest galactic supernova remnant G1. 9+ 0.3. *Astrophys. J. Lett.* **837**, L7 (2017).
15. Gower, A. C. & Hutchings, J. B. A precessing relativistic jet model for 3C 449. *Astrophys. J.* **258**, L63–L66 (1982).
16. Dunn, R. J. H., Fabian, A. C. & Sanders, J. S. Precession of the super-massive black hole in NGC 1275 (3C 84)? *Mon. Not. R. Astron. Soc.* **366**, 758–766 (2006).
17. Pringle, J. E. Self-induced warping of accretion discs. *Mon. Not. R. Astron. Soc.* **281**, 357–361 (1996).
18. Nixon, C. & King, A. Do jets precess… or even move at all? *Astrophys. J. Lett.* **765**, L7 (2013).
19. Kharb, P. et al. Double-peaked emission lines due to a radio outflow in KISSR 1219. *Astrophys. J.* **846**, 12 (2017).
20. Beck, S. C., Jean, L. T. & Michelle Consiglio, S. Dense molecular filaments feeding a starburst: ALMA maps of CO (3–2) in Henize 2-10. *Astrophys. J.* **867**, 165 (2018).
21. Lee, M. G. et al. Optical spectroscopy of supernova remnants in M81 and M82. *Astrophys. J.* **804**, 63 (2015).
22. Trump, J. R. et al. Accretion rate and the physical nature of unobscured active galaxies. *Astrophys. J.* **733**, 60 (2011).
23. Reines, A. E. et al. A new sample of (wandering) massive black holes in dwarf galaxies from high-resolution radio observations. *Astrophys. J.* **888**, 36 (2020).
24. Molina, M. et al. Outflows, shocks, and coronal line emission in a radio-selected AGN in a dwarf galaxy. *Astrophys. J.* **910**, 5 (2021).
25. Allen, M. G. et al. The MAPPINGS III library of fast radiative shock models. *Astrophys. J. Suppl. Ser.* **178**, 20 (2008).
26. Silk, J. & Norman, C. Global star formation revisited. *Astrophys. J.* **700**, 262 (2009).
27. Silk, J. Unleashing positive feedback: linking the rates of star formation, supermassive black hole accretion, and outflows in distant galaxies. *Astrophys. J.* **772**, 112 (2013).
28. Penny, S. J. et al. SDSS-IV MaNGA: evidence of the importance of AGN feedback in low-mass galaxies. *Mon. Not. R. Astron. Soc.* **476**, 979–998 (2018).
29. Trump, J. R. et al. Spectropolarimetric evidence for radiatively inefficient accretion in an optically dull active galaxy. *Astrophys. J.* **732**, 23 (2011).
30. Santoro, F. et al. AGN-driven outflows and the AGN feedback efficiency in young radio galaxies. *Astron. Astrophys.* **644**, A54 (2020).

Methods

The controversy of massive black hole or supernova remnant

In recent years, evidence has been mounting for a massive black hole powering a low-luminosity AGN at the centre of Henize 2-10 (refs. [6–9]), although a supernova remnant has been proposed as an alternative by some authors[10,11]. As discussed in the Article, the radio and X-ray point source luminosities are consistent with both. A recent study[10] argues for a supernova remnant based on their findings that the X-ray spectrum is better fit by a hot plasma model (typically used for supernova remnants) than a power-law model (typically used for luminous AGNs). However, the soft X-ray spectrum of the nuclear source in Henize 2-10 does resemble massive black holes accreting at very low Eddington fractions[31] including Sagittarius A* in the Milky Way[32]. Another study using ground-based spectroscopy favoured a supernova-remnant origin for the central source based on a lack of any AGN ionization signatures[11]. However, the ground-based observations used in that work had an angular resolution of approximately 0.7", which is not sufficient to cleanly isolate the weakly accreting black hole from nearby young (<5 Myr) massive ($M_\star \sim 10^5 M_\odot$) star clusters that dominate the line ratios at this relatively course angular resolution.

There are other observational results to consider regarding the origin of the nuclear radio and/or X-ray source in Henize 2-10. For example, a recent study using adaptive optics integral field spectroscopy provides evidence for gas excited by an AGN and an enhanced stellar velocity dispersion at the location of the nuclear source consistent with an approximately $10^6 M_\odot$ black hole, favouring the low-luminosity AGN interpretation[9]. There is also evidence for moderately significant variability on hour-long timescales in the X-ray light curve, which is incompatible with a supernova remnant[8,10]. Moreover, it is reasonable to expect that Henize 2-10 hosts a massive black hole because its overall structure resembles an early-type galaxy (albeit with a central starburst) and its stellar mass may be as high as $M_\star \sim 10^{10} M_\odot$ (ref. [33]), a regime in which the black-hole occupation fraction is near unity[34]. The central starburst complicates the identification of the weakly accreting black hole, yet a variety of multiwavelength observational results taken collectively strongly support its presence. These results are summarized in Extended Data Table 1. A highly sub-Eddington massive black hole is consistent with all of the observations, including the work presented here, whereas a supernova remnant is not. The present study not only adds to the evidence for a massive black hole in Henize 2-10, but it also demonstrates that a bipolar outflow from the black hole is enhancing and/or triggering star formation in its vicinity.

STIS observations and data reduction

Spatially resolved spectroscopic observations of the nuclear regions of the dwarf starburst galaxy Henize 2-10 were obtained using the STIS instrument on the HST. We obtained observations with two slit orientations. The first was aligned with the quasi-linear ionized gas structure identified by Reines et al.[6] and covers the central radio and/or X-ray source and the bright knot of ionized gas to the east. We refer to this as the east–west (EW) orientation. The second slit orientation was placed perpendicular to the EW observation at the location of the central radio and/or X-ray source. We refer to this as the north–south (NS) orientation. The candidate AGN itself was too faint to acquire directly, and therefore we used a target acquisition with an offset from a bright point source 7.9" to the southeast.

Spectra were taken with the G750M and G430M gratings providing medium spectral resolution (R ~ 5,000–6,000) coverage of key optical emission lines. The central wavelengths were set at 6,581 Å and 4,961 Å for the G750M and G430M gratings, respectively. At each slit orientation, two orbits were spent in G430M and one orbit in G750M. The observations were taken with a two-point dither pattern with CR-SPLITS (multiple exposures taken to aid in cosmic ray rejection) at each position to help eliminate cosmic rays. The calibrated dithered images were combined and had a spatial resolution of approximately 0.1", which corresponds to a physical scale of approximately 4 pc at the distance of Henize 2-10 (approximately 9 Mpc).

Emission line fitting

Before we fitted emission lines in the spectra, we first modelled and removed the continuum. The reduced spectra were continuum-subtracted by masking emission-line regions and fitting a low-order polynomial to the continuum in each row in the spatial dimension. A low-order polynomial was used given the lack of absorption features in the spectra. We did, however, consider the potential effect of stellar absorption lines on our measurements and found that the absorption line strengths were negligible compared with the emission-line strengths. Scaling a Starburst99 (ref. [35]) model for a 4 Myr stellar population (see the 'Star cluster ages' section below) to our observed spectra, we found that the flux of Hα absorption is smaller by a factor of 61 than the Hα emission and the flux of the Hβ absorption is smaller by a factor of 7 than the Hβ emission at the location of the central source. Accounting for this absorption has a negligible effect on the line ratios of the nuclear source and does not influence the classifications based on the diagnostic diagrams.

Once the spectra were continuum-subtracted, we fitted each emission line of interest with a linear combination of Gaussian profiles to characterize the flux and estimate the kinematic properties along the spatial dimension of each slit. The fitting was done using lmfit[36], a non-linear least-squares curve fitting package in Python. We fitted each emission line with up to two Gaussian components when needed. To determine if a second Gaussian component was warranted, we required that the flux of both components be greater than the 3σ error of the flux. This process is performed row by row in the spatial direction along each slit for the emission lines of interest. During this process we fitted the Hβ, [O III]5007, Hα, [N II]6548/6583 and [S II]6716/6731 emission lines. We fitted the Hα and [N II] lines simultaneously, fixing the spacing between [N II] Gaussian components to their corresponding components in the Hα emission line to laboratory values. Additionally, we tied the widths of [N II] components and fixed the flux ratio of the [N II] lines to the laboratory value of 1:2.96. Similarly, the two [S II] emission lines were fitted simultaneously, with the spacing between Gaussian components of the two lines held fixed, and the widths of the Gaussian components were tied together.

We also fitted [O I]6300 in the spectra of the nuclear source and the eastern star-forming region, but the line was too weak to be detected all along the slits. As the [O I]6300 line has a complex profile at the location of the black hole, with possible double-peaked narrow lines and a much broader component than the other emission lines, we confirmed that this was not due to an artefact in the data. In Extended Data Fig. 1, we show close-up views of the raw two-dimensional (2D) spectra along the EW slit position. The two images correspond to the two dithered subexposures offset by 7.5 pixels. The broad [O I] line at the location of the central source is seen in both images at different positions on the detector (indicated by white circles). Note that the locations of hot pixels do not change between the two images. In Extended Data Fig. 2 we also show the final reduced 2D image with the subexposures combined. The broad, double-peaked nature of the [O I] line is clearly visible. We also note that [O I] is similarly broadened in the nuclear spectrum extracted from the NS slit position, although there is not an obvious double-peaked narrow line component (Fig. 2). In any case, broadened [O I] is clearly detected at the location of the nuclear source in both slit positions indicating an outflow of the order of approximately 500 km s^{-1}.

Gas density

We estimate the electron density, n_e, using the density sensitive line ratio [S II]6716/6731 (ref. [37]). This ratio is sensitive to electron densities in the range of approximately 10^2–10^4 cm^{-3}. Along the EW slit

orientation, we find a range of $n_e \sim 10^{2.5}$–10^4 cm^{-3}, indicating a relatively high-density gas (Extended Data Fig. 3). These density estimates are in general agreement with the gas densities predicted by the Allen et al.[25] shock and shock+precursor models in the central regions of Henize 2-10 as described in the next section.

Emission line diagnostics and photoionization and shock models

To understand the ionization mechanisms in the central regions of Henize 2-10 we compared our emission-line measurements in various regions with photoionization and shock models. In addition to the central radio and X-ray source, we identified seven regions of interest, as shown in Extended Data Fig. 4, which serve to provide a spatially resolved picture of the kinematics and ionization conditions in the central regions of Henize 2-10. The extraction regions taken along the EW slit orientation were chosen to correspond with the emission features seen in the Hα and I-band imaging from HST (young star clusters and knots of ionized gas) and the features seen in the STIS spectroscopy (broad emission and double peaks).

We first used the standard emission-line diagnostic diagrams described by Baldwin et al.[38] and Veilleux et al.[39] that have been expanded on and summarized in Kewley et al.[40]. An accreting black hole will produce a much harder continuum than is emitted by hot stars, and these diagrams take advantage of this fact by comparing strong emission-line ratios that are close together in frequency to mitigate reddening effects. In this study we utilized widely used emission-line diagnostic diagrams that take [O III]/Hβ versus [N II]/Hα, [S II]/Hα and [O I]/Hα (Extended Data Fig. 5). In the [N II]/Hα diagram, line-emitting galaxies separate into a V-shape[40] with star-forming galaxies occupying the left-most plume, whereas AGNs occupy the right branch of galaxies. These regions are quantified by an empirical division between H II regions and emission from AGNs developed by Kauffmann et al.[41]. The 'composite' region between this empirical division and the theoretical maximum starburst line from Kewley et al.[42] indicates that there is probably significant emission form both H II regions and AGNs. Like the [N II]/Hα diagram, the [S II]/Hα and [O I]/Hα diagrams provide diagnostics for differentiating between emission from H II regions and AGNs. These two diagrams add a dividing line to distinguish between emission from Seyferts and low ionization nuclear emission regions (LINERs). LINER emission can be generated both by shocks and by very hard AGN spectra, and determining the primary ionization mechanism can be complicated[37]. It should be noted that even though these diagnostic diagrams are useful for identifying regions dominated by luminous AGNs, they have limitations and can yield ambiguous results for (or completely miss) massive black holes accreting at very low Eddington ratios, such as the one in Henize 2-10. Indeed, non-stellar ionization is clearly indicated in the [O I]/Hα diagram at the location of the nuclear source, but this is not so for the other diagnostic diagrams (see the discussion in paragraph six of the main paper). Extended Data Fig. 5 shows the [O III]/Hβ versus [N II]/Hα, [S II]/Hα and [O I]/Hα diagnostic diagrams for the various extraction regions along the EW slit.

In addition to the diagnostic diagrams discussed above, we also investigated whether the ionization conditions found in the central regions of Henize 2-10 can be explained by mechanical excitation from shocks. To investigate this, we used the ionization models of shock and shock+precursor emission developed by Allen et al.[25]. These models provide emission-line fluxes for ionization from a pure shock (possibly driven by an outflow from an AGN or by regions of intense star formation), in which the gas is collisionally ionized, or a shock+precursor in which ionizing photons produced in the shock-heated gas travel upstream and ionize the gas before the shock reaches it. We explored models with a variety of electron densities (0.01–1,000 cm^{-3}), shock velocities (100–600 km s^{-1}) and transverse magnetic field strengths (0.01–32 μG). These are shown in Extended Data Figs. 6 and 7.

The emission-line ratios from the nuclear source are best described by the shock+precursor models with a low shock velocity (100–250 km s^{-1}), a high-density gas (n = 1,000 cm^{-3}) and a low transverse magnetic field parameter (b = 0.01–1 μG) (Extended Data Figs. 6 and 7). Shock+precursor models are thought to be a good description for AGN+outflow emission. Along the filament (extraction regions 2–5), the line ratios are explained well by a low velocity shock or shock+precursor model (approximately 200 km s^{-1}) in a high-density ($n_e \sim$ 1,000 cm^{-3}) gas with a transverse magnetic field parameter in the range of 1–10 μG. This is consistent with a scenario in which the central black hole is driving a bipolar outflow that shocks the gas and dominates the ionization conditions along the filament.

At the region of intense star formation located approximately 70 pc to the east of the black hole, we observed strong emission lines including a secondary, blue-shifted kinematic component. To properly fit the emission lines in this region, an additional Gaussian component was added (Fig. 3). The separation of this component was determined using the [S II] emission-line region in which the secondary peak was most clearly resolved. We found that the secondary peak is offset from the primary peak by 154 km s^{-1} and we used this value when fitting the other emission-line regions in which the secondary peak is not as well resolved. When comparing with the shock(+precursor) models, we found that the [N II]/Hα diagram indicates a low shock velocity (100–250 km s^{-1}) in a high-density gas (n = 1,000 cm^{-3}) with a low transverse magnetic field parameter (b = 0.01–1 μG) (Extended Data Figs. 6 and 7). The [S II]/Hα diagram shows that the primary emission peak is inconsistent with emission from shocks or shocks+precursor models. This indicates that the primary emission peak at this location is primarily due to star formation. The secondary emission peak is consistent with shock+precursor models for the low-velocity, high-density conditions, indicating that this kinematically distinct emission component is dominated by a shock+precursor from the AGN-driven outflow.

Emission from extraction regions 6 and 7 (that is, the western star-forming region) is not consistent with any shock or shock+precursor models, which is in agreement with their location in the H II region of the Baldwin–Phillips–Terlevich (BPT) diagram. The line ratios are dominated by star formation in this region.

Star cluster ages

We estimated the ages of the young stellar clusters that fall within the EW slit from their Hα and Hβ equivalent widths. To ascertain ages from these equivalent widths we used simple stellar population models from Starburst99 (ref. [35]). We used models from version 7.1 with solar metallicity (appropriate for the central regions of Henize 2-10; ref. [43]), an instantaneous burst of 10^4 $M_\odot$ with a Kroupa initial mass function (0.1–100 $M_\odot$), the Geneva evolutionary tracks with high mass loss and the Pauldrach–Hillier atmospheres.

At the location of the young stellar clusters in the eastern star-forming region (region 1 in Extended Data Fig. 4) we found an equivalent width of 478 Å and 70 Å for Hα and Hβ, respectively. These both give stellar population age estimates of approximately 4.3 Myr, which is in good agreement with previous estimates of the ages of other young star clusters in the region[44]. The ages of these clusters are larger than the crossing time for the AGN-driven outflow (approximately 0.3 Myr), based on the minimum outflow velocity measured from emission-line spectra (approximately 200 km s^{-1}) and the distance between the AGN and the eastern star-forming knot (approximately 70 pc). Therefore, the timescales enable the AGN-driven outflow to have triggered and/or enhanced the formation of star clusters in the eastern star-forming knot.

The EW slit orientation also passes through a young star cluster in region 3. At this location we found equivalent widths of 212 Å and 41 Å for Hα and Hβ, respectively, both indicating an age of approximately 5.2 Myr for the stellar cluster. Finally, region 6 in the western star-forming region had Hα and Hβ equivalent widths of 1,092 Å and

196 Å, respectively. These equivalent widths indicate the stellar clusters have ages $\lesssim$3 Myr.

Bipolar outflow model

Here we provide a derivation of the model used to describe a precessing bipolar outflow emanating from the nuclear radio and X-ray source, which can explain the coherent velocity pattern seen in the central approximately 120 pc of the EW orientation observations (Fig. 3). In this model, we align the EW slit orientation with the z axis and assume the outflow precesses about this axis with a small angle θ and an angular precession frequency ω. If the gas being ejected by the outflow has velocity v_0, and we orient the x axis to be in the direction of the observer, then the radial (Doppler-shifted) velocity found at the location of the AGN as a function of time will be given by

$$v_r(t) = v_x(t) = v_0 \sin(\theta) \sin(\omega t + \gamma),$$

where γ represents a phase shift that accounts for small asymmetries in the outflow profile, which are not explicitly modelled here (see Extended Data Fig. 8 for an illustration of our model).

To find the radial velocity as a function of distance (z) along the slit axis, we must consider what angle the outflow made with the (line-of-sight) x axis when the gas at distance z was emitted. As this angle is time dependent as the outflow precesses, the line-of-sight velocity of the gas will depend on the orientation of the outflow at some time t_0 in the past. The time that has passed since the gas at distance z was ejected by the outflow is determined by the z velocity of the gas. Owing to the symmetry of the model about the z axis, the z component of the gas velocity will be time independent and only depend on the angle of the outflow with the z axis,

$$v_z = v_0 \cos(\theta).$$

The time, t_0, for the gas to reach a distance z along the slit is then given by

$$t_0 = \frac{z}{v_0 \cos(\theta)}.$$

We are then able to find an expression for $v_r(z)$ by evaluating the expression for $v_r(t)$ at the time $-t_0$:

$$v_r(z) = v_0 \sin(\theta) \sin\left(\gamma - \frac{\omega}{v_0 \cos(\theta)} z\right)$$

To fit this model to the data we require a rough estimate of the bulk outflow velocity, v_0. We estimate this parameter using W80, the velocity interval containing 80% of the line flux, of the broad emission seen at the location of the candidate AGN. We find W80 $\approx$ 200–500 km s^{-1} based on measurements of the [O III]5007 and [O I]6300 lines at the location of the candidate AGN. This enables us to determine the best-fit angle of precession, θ, and the frequency of precession, $f = \omega/2\pi$, to be in the ranges

$$\theta = 2.4° - 6.1°, \; f = 3.0 - 7.5 \text{ revolutions Myr}^{-1}$$

where the larger angle of precession and smaller frequency of precession correspond to lower outflow velocities. We found consistent results when using the Doppler shift profile of Hα, Hβ and [O III] emission lines to fit the model derived above (the results using the [O III] emission line are shown in Fig. 3). The Doppler shift profile can be coherently traced out to 50–60 pc on either side of the candidate AGN, and most definitively out to the bright eastern star-forming region, after which the Doppler shifts of the emission lines show no coherent pattern further along the slit. The coherent velocity structure found over 100 pc is inconsistent with a young supernova remnant as the origin of the central compact radio and X-ray source in Henize 2-10, which provides further motivation that a low-luminosity AGN is driving the outflow.

These results are roughly consistent with the jet parameters derived in other studies in which precessing or reorienting jet models have been applied. The long precession period we observed (approximately 200,000 years) is shorter by a factor of a few than those predicted by Dunn et al.[16], Nawaz et al.[45] and Cielo et al.[46], but longer by a factor of a few than those predicted by Gower et al.[15] when jet precession is invoked to explain the complex bending and knotting seen in large radio jets.

Data availability

The spectroscopic data analysed in this study are available from the Mikulski Archive for Space Telescopes (MAST) at https://archive.stsci.edu/.

31. Constantin, A. et al. Probing the balance of AGN and star-forming activity in the local universe with ChaMP. *Astrophys. J.* **705**, 1336 (2009).
32. Baganoff, F. K. et al. Chandra X-ray spectroscopic imaging of Sagittarius A* and the central parsec of the galaxy. *Astrophys. J.* **591**, 891 (2003).
33. Nguyen, D. D. et al. Extended structure and fate of the nucleus in Henize 2-10. *Astrophys. J.* **794**, 34 (2014).
34. Greene, J. E., Strader, J. & Ho, L. C. Intermediate-mass black holes. *Annu. Rev. Astron. Astrophys.* **58**, 257–312 (2020).
35. Leitherer, C. et al. Starburst99: synthesis models for galaxies with active star formation. *Astrophys. J. Suppl. Ser.* **123**, 3 (1999).
36. Newville, M., Stensitzki, T., Allen, D. B. & Ingargiola, A. LMFIT: non-linear least-square minimization and curve-fitting for Python version 0.8.0. *Zenodo* https://doi.org/10.5281/zenodo.11813 (2014).
37. Osterbrock, D. E., and Ferland, G. J. *Astrophysics of Gas Nebulae and Active Galactic Nuclei* (University Science Books, 2006).
38. Baldwin, J. A., Phillips, M. M. & Terlevich, R. Classification parameters for the emission-line spectra of extragalactic objects. *Publ. Astron. Soc. Pac.* **93**, 5 (1981).
39. Veilleux, S. & Osterbrock, D. E. Spectral classification of emission-line galaxies. *Astrophys. J. Suppl. Ser.* **63**, 295–310 (1987).
40. Kewley, L. J. et al. The host galaxies and classification of active galactic nuclei. *Mon. Not. R. Astron. Soc.* **372**, 961–976 (2006).
41. Kauffmann, G. et al. The host galaxies of active galactic nuclei. *Mon. Not. R. Astron. Soc.* **346**, 1055–1077 (2003).
42. Kewley, L. J. et al. Theoretical modeling of starburst galaxies. *Astrophys. J.* **556**, 121 (2001).
43. Martín-Hernández, N. L. et al. High spatial resolution mid-infrared spectroscopy of the starburst galaxies NGC 3256, II Zw 40 and Henize 2-10. *Astron. Astrophys.* **455**, 853–870 (2006).
44. Chandar, R. et al. The stellar content of Henize 2-10 from space telescope imaging spectrograph ultraviolet spectroscopy. *Astrophys. J.* **586**, 939 (2003).
45. Nawaz, M. A. et al. Jet–intracluster medium interaction in Hydra A–II. The effect of jet precession. *Mon. Not. R. Astron. Soc.* **458**, 802–815 (2016).
46. Cielo, S. et al. Feedback from reorienting AGN jets-I. Jet–ICM coupling, cavity properties and global energetics. *Astron. Astrophys.* **617**, A58 (2018).

Acknowledgements We are grateful to M. Molina for useful discussions regarding shocks. We also thank M. Whittle and K. Johnson for their assistance with the HST/STIS proposal while A.E.R. was a graduate student at the University of Virginia, and for subsequent discussions. Support for Program number HST-GO-12584.006-A was provided by NASA through a grant from the Space Telescope Science Institute, which is operated by the Association of Universities for Research in Astronomy, Incorporated, under NASA contract NAS5-26555. A.E.R. also acknowledges support for this work provided by NASA through EPSCoR grant number 80NSSC20M0231. Z.S. acknowledges support for this project from the Montana Space Grant Consortium.

Author contributions Z.S. reduced and analysed the STIS data and compared the results with models. A.E.R. led the HST/STIS proposal and helped with the data reduction. Both authors worked on the interpretation of the results and the writing of the paper.

Competing interests The authors declare no competing interests.

Additional information

Supplementary information The online version contains supplementary material available at https://doi.org/10.1038/s41586-021-04215-6.

Correspondence and requests for materials should be addressed to Zachary Schutte.

Peer review information *Nature* thanks Rogério Riffel and the other, anonymous, reviewer(s) for their contribution to the peer review of this work. Peer reviewer reports are available.

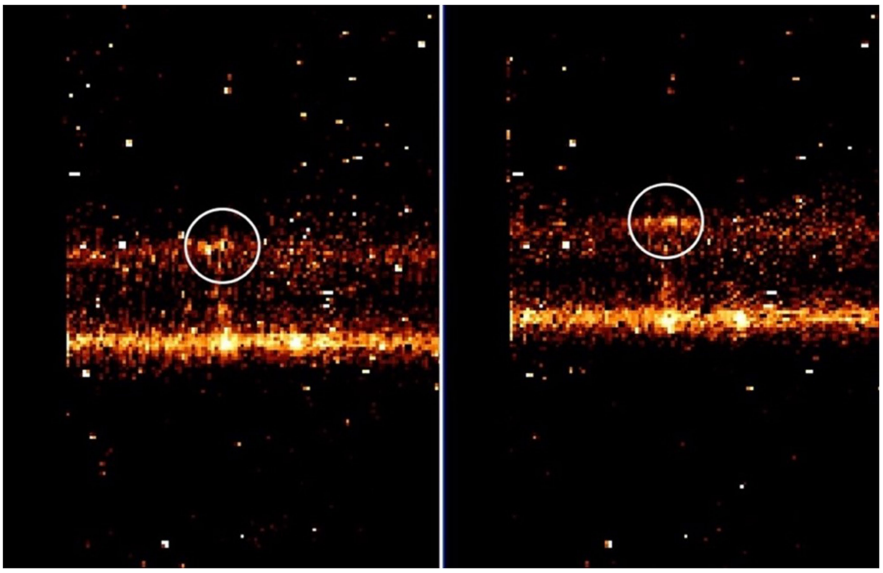

Extended Data Fig. 1 | Raw 2D spectra showing the [OI]6300 emission line at the location of the nucleus in the EW slit orientation. The location of the nucleus is indicated by white circles and the two images correspond to the two dithered sub-exposures.

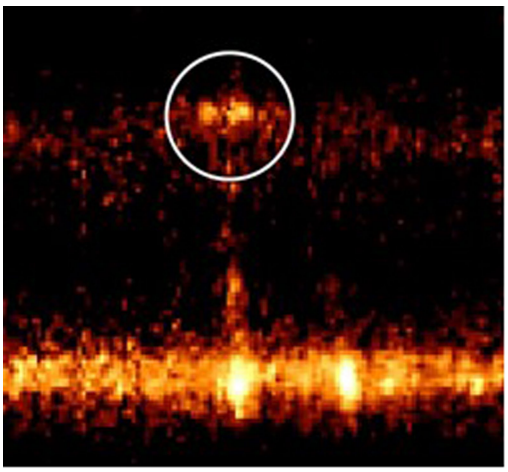

Extended Data Fig. 2 | Combined 2D spectra showing the [OI]6300 emission line at the location of the nucleus in the EW slit orientation. Same as Extended Data Fig. 1 but showing the reduced 2D image with the dithered sub-exposures combined.

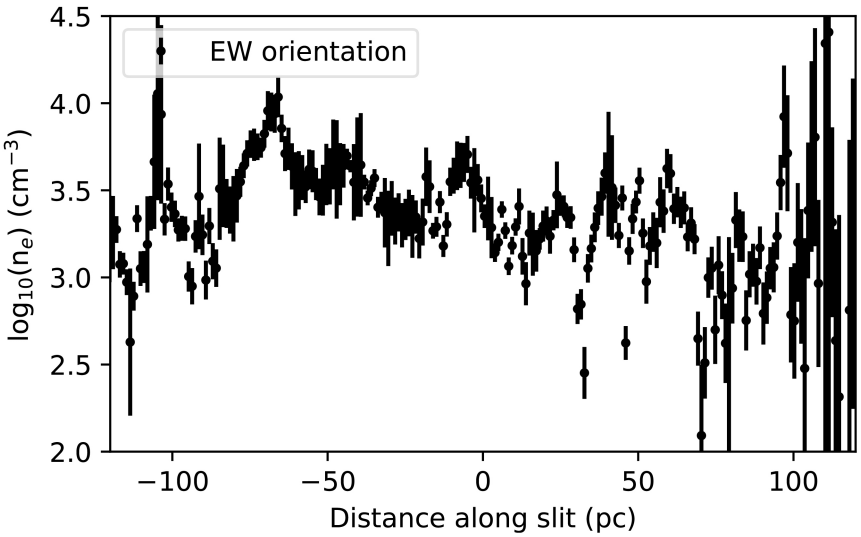

Extended Data Fig. 3 | The electron density, n_e, along the EW slit orientation. We measure the electron density along the EW slit from the ratio of [SII]6716/[SII]6731 and find the electron density ranges from $\sim 10^{2.5} - 10^4\,cm^{-3}$, which is within the range the [SII] ratio is sensitive to density. The high densities are consistent with those predicted by optical emission line diagnostics derived from the Allen et al.[25] shock models.

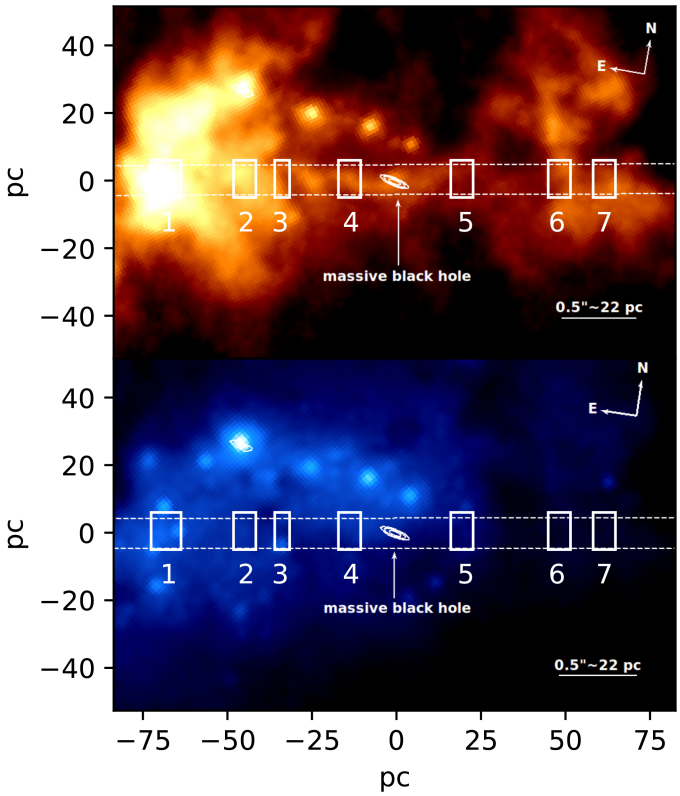

Extended Data Fig. 4 | The spatial extraction regions taken along the EW slit orientation. We place these regions on optical emission line diagnostic diagrams (Extended Data Figs. 5–7). Top panel: the extraction regions are shown on the narrow band Hα + continuum image from HST to highlight the ionized gas features that several of the spatial extractions probe. Bottom panel: the extraction regions are shown on the archival 0.8 micron HST image, showing young star clusters that the EW slit orientation passes through.

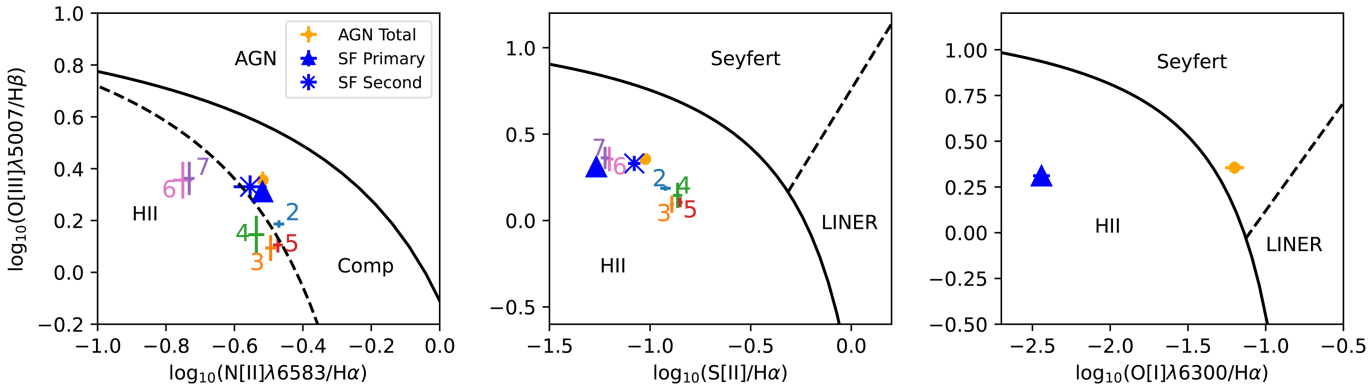

Extended Data Fig. 5 | Narrow emission line diagnostic diagrams showing various extraction regions along the EW slit orientation (see Extended Data Fig. 4). The nucleus (yellow point) falls in the Seyfert region of the [OI]/Hα diagram. The young star-forming region ~70 pc to the east of the low-luminosity AGN is depicted with a blue triangle and star for the primary emission line component and the blue-shifted secondary component, respectively. [OI] is not detected in all of the regions.

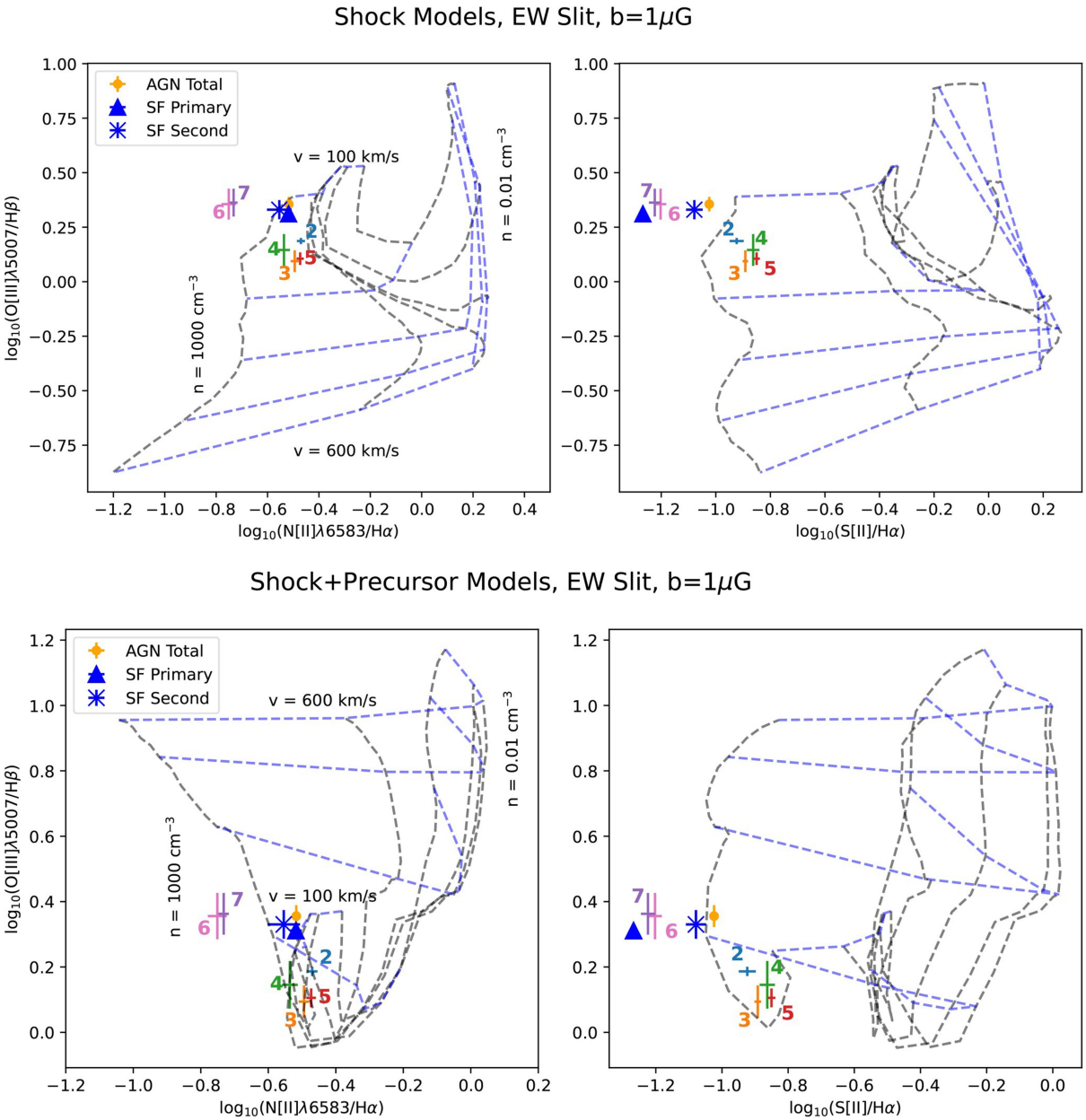

Extended Data Fig. 6 | Optical emission line diagnostics from the shock and shock+precursor models with varying gas density. We place the spatial extractions from the EW slit orientation shown in Extended Data Fig. 4 on a grid of shock excitation models (presented in Allen et al.[25] with varying gas density (n = 0.01-1000 cm^{-3}) and shock velocity (v = 100-600 km/s). We fix the transverse magnetic field to be b = 1μG and the assume solar metallicity.

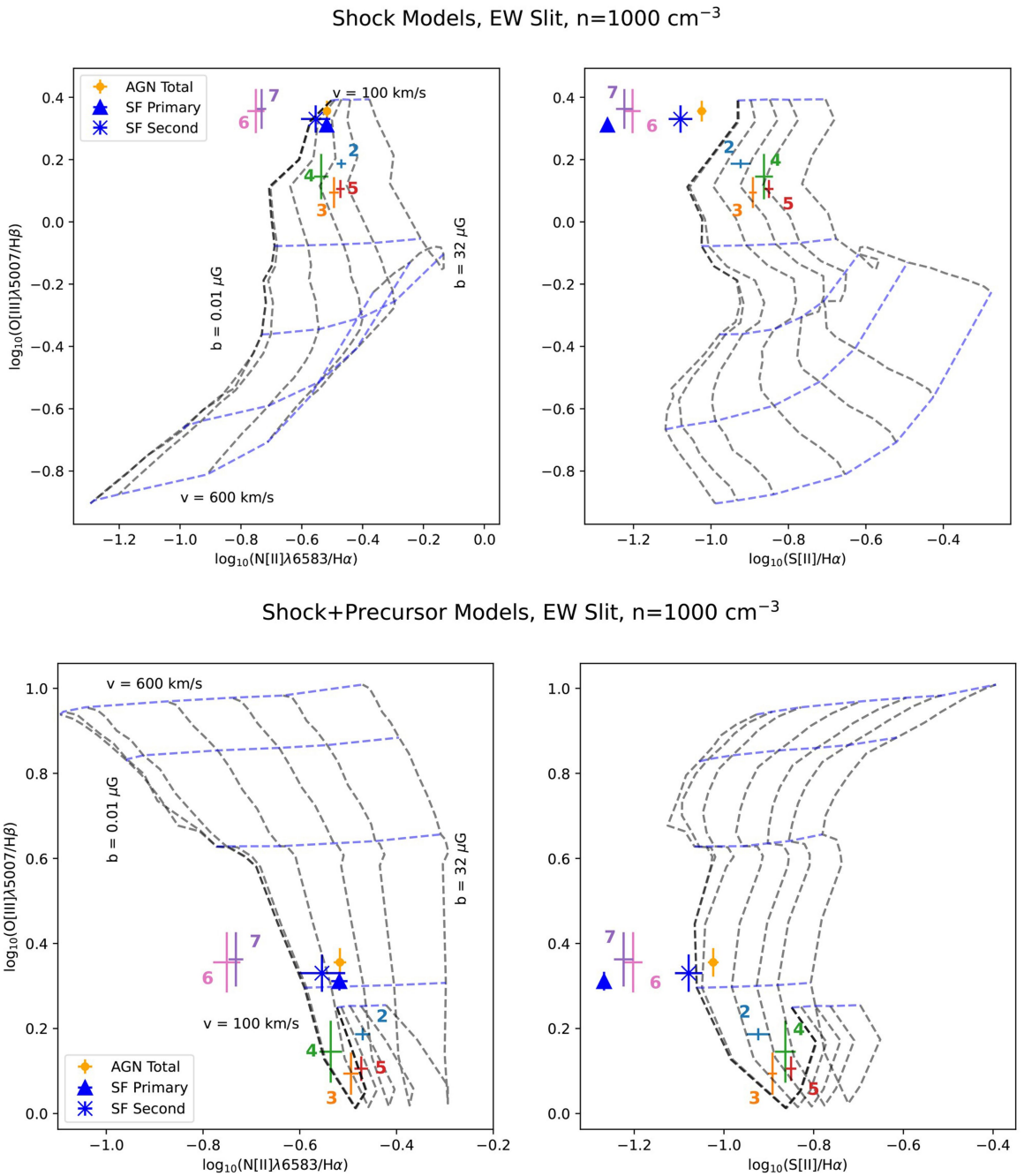

Extended Data Fig. 7 | Optical emission line diagnostics from the shock and shock+precursor models with varying magnetic field. The models (presented in Allen et al.[25]) are shown as a grid with dashed blue lines indicating constant shock velocity and dashed black lines indicating constant transverse magnetic field. For these models, the density is fixed to n = 1000 cm^{-3} and the transverse magnetic field parameter is allowed to vary from b = 0.01-32 μG.

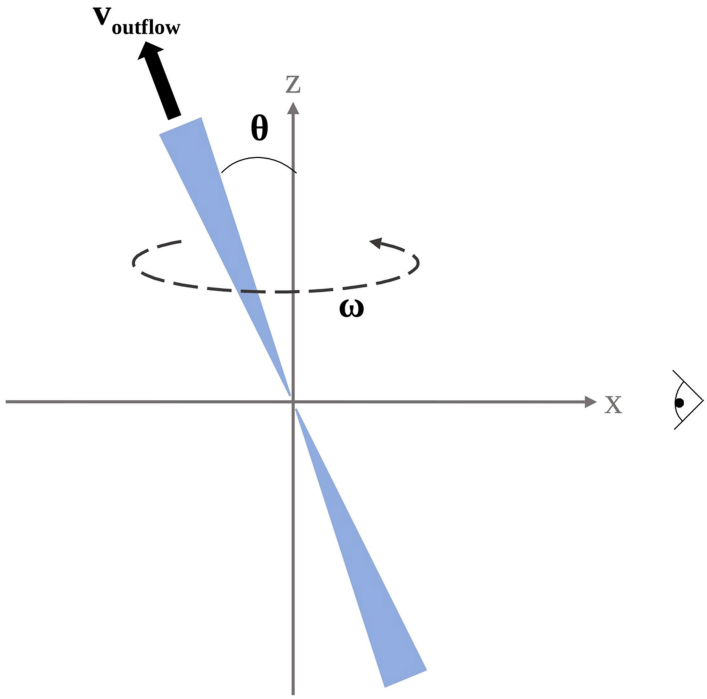

Extended Data Fig. 8 | A diagram of the toy model of the bipolar outflow generated by the low-luminosity AGN in Henize 2-10. Our simple model depends on the outflow velocity of the ionized gas ($v_{outflow}$), the angle the outflow makes with its precession axis (θ) and the angular frequency with which the outflow precesses (ω). Similar models have been used to describe the bending seen in large radio jets[15,16].

Extended Data Table 1 | Summary of observational results regarding the nature of the nucleus in Henize 2-10

Observations	Consistent with massive black hole?	Consistent with supernova remnant?	Notes and References
Nuclear, non-thermal radio point source with $L_R \sim 4 \times 10^{35}$ erg/s	yes	yes	• Nuclear, non-thermal point source detected with the VLA (Johnson et al. 2003; Reines et al. 2011). • VLBI observations confirm non-thermal origin and constrain the nuclear radio source to be $\lesssim 3 \times 1$ pc. If SNR, size and luminosity imply it must be very young (Reines & Deller 2012).
Spatially coincident nuclear X-ray point source with $L_X \sim 10^{38}$ erg/s	yes	yes	• Nuclear X-ray point source detected with *Chandra* that is spatially coincident with radio source. If massive BH, X-ray luminosity implies highly sub-Eddington accretion, which is consistent with soft X-ray spectrum. An X-ray binary is ruled out by the high luminosity of the compact radio source (Reines et al. 2016). • X-ray spectrum also consistent with SNR (Hebbar et al. 2019)
X-ray variability on hr-long timescales	yes	no	• X-ray light curve from 160 ks *Chandra* observation exhibits moderately significant variability (a factor of ~2; Reines et al. 2016). Probability of non-variable light curve producing the signal is 3% (Hebbar et al. 2019). • Tentative detection of ~9-hr periodicity in the variable light curve (Reines et al. 2016).
Enhanced stellar velocity dispersion at location of nuclear source	yes	no	• Stellar velocity dispersion map from near-IR IFU observations reveals enhancement of ~7 km/s at position of nuclear source, consistent with a BH mass of $\sim 1.5 \times 10^6$ M_{sun} (Riffel et al. 2020). This is in line with expectations given the stellar mass of Henize 2-10 ($\sim 10^{10}$ M_{sun}, Nguyen et al. 2014). • No detectable star cluster at location of the central source (Reines et al. 2011). This is in contrast to a weaker, more extended off-nuclear VLBI source, which is co-spatial with the most luminous super star cluster in Henize 2-10, and is a likely SNR (Reines & Deller 2012).
Gas excitation and ionization conditions	yes	?	• Enhanced near-IR [Fe II]/Brγ ratio consistent with accreting BH or supernova driven shocks (Riffel et al. 2020; Cresci et al. 2010). • Near-IR H_2 line ratios consistent with AGN photoionization (Riffel et al. 2020). • Optical line ratios from ground-based spectra dominated by star formation (Cresci et al. 2017). • HST/STIS observations show non-stellar emission-line ratios involving [OI]. SNRs have log [SII]/Hα > -0.5, which is not seen in the STIS spectrum of the nuclear source (**this work**).
Gas kinematics and morphology	yes	no	• Spectroscopy at high spatial resolution shows broadened near-IR and optical emission lines at the location of the central source (Riffel et al. 2020 and **this work**). In particular, [OI]6300 has a FWHM of ~500 km/s indicating an outflow from the central source (**this work**). Very young SNRs typically have broad lines with widths on the order of thousands of km/s. • HST/STIS spectroscopy along a ~150 pc-long ionized gas filament centered on the nuclear source (seen in Hα imaging with HST) exhibits a coherent sinusoid-like pattern in the Doppler shifted velocities. The position-velocity data is well-fit by a simple model of a precessing bipolar outflow from a massive BH, and is incompatible with a SNR (**this work**).

A highly sub-Eddington massive black hole is consistent with all the available observations including new results presented here, while a supernova remnant is not.